Progress In Electromagnetics Research, Vol. 125, 21–35, 2012

PLANAR SYMMETRIC NORMAL AND COMPLEMENTARY THREE-RESONANCE RESONATORS IN TERAHERTZ BAND

Y.-X. Zhang*, S. Qiao, Z. Tao, W. Ling, and S. Liu

Terahertz Science and Technology Research Center, University of Electronic Science and Technology of China, Chengdu 610054, China

Abstract—Metamaterials are artificially structured electromagnetic materials which can lead to the realization of phenomena that cannot be obtained with natural materials. In the terahertz frequency regime, metamaterials have distinguished performance and open up a new way to design and construct the functional devices. Based on the structure of metamaterials, planar symmetric normal and complementary three-resonance resonators in Terahertz band are proposed in this paper. Simulation and experimental study have been carried out. The results show that the proposed structure has three distinct and strong resonant bands in THz regime and that symmetric normal structure and complementary structure can realize the three stop-resonances and pass-resonances respectively. For the well-separating of different resonances in the terahertz band, these symmetric three-passband and three-stopband resonators will be used in the design of multiband terahertz devices.

1. INTRODUCTION

Artificial electromagnetic structures, called metamaterials, can be engineered to exhibit exotic electric and magnetic properties not realizable in nature [1–16]. Nowadays, terahertz science and technology becomes an attractive research area. However, in terahertz regime, most natural materials cannot be utilized for controlling the radiation. The introduction of terahertz metamaterials is believed to be an important step on the path of furthering advance terahertz research and development, so metamaterials are of particular interest in this frequency band. Owing to their customizable electromagnetic

Received 21 December 2011, Accepted 6 February 2012, Scheduled 14 February 2012

* Corresponding author: Ya-Xin Zhang (zhangyaxin@uestc.edu.cn).

properties, metamaterials can provide sufficiently useful characteristics and a variety of terahertz components that have been proposed, including terahertz filters, perfect absorbers, quarter-wave plates, modulators, molecular sensors, etc. [17–25].

Recently, terahertz single-band and dual-band metamaterials have already been fabricated and experimentally proved [25–33]. For instance, dual-resonance dynamical electric and magnetic metamaterials [27–29], dual-band planar electric metamaterials in the terahertz regime [25–27] and a dual-band and three-band SRR metamaterials in micro-band [30, 31], etc. have been proposed and presented. Moreover, in recent years, complementary metamaterial structures, whose resonant characteristics are opposite to those of normal ones, have also been studied [34–36]. Numerous papers experimentally verify the resonant characteristics and explain the resonant phenomena, such as the exploration of six different complementary structures with one resonant frequency [34] and the analysis of resonances in SRR with one or two resonant peak [35]. It is safe to say that the design and fabrication of multi-resonant metamaterials are potentially useful in the multiple band-pass or band-stop filter, switch, modulator and so on. So it seems to be attractively applicable in THz band. However, in THz regime, only a few papers present study on the multi-resonance (≥ 3), and most papers concentrated in two-resonance structure. As a step towards frequency agile or broadband THz materials and devices, based on the structures of metamaterials, the symmetric normal and complementary three-resonance resonators are proposed in this paper. Different from the asymmetric one, in the symmetric structure there is a pair of resonant circuits (mirror symmetric) for one resonant frequency, so the resonant intensity is stronger and frequency resolution better. Therefore, the complementary symmetric structure is very conductive to realize the three pass-resonances.

Here, we present the study of pass-resonant and stop-resonant resonators, and each of them has three distinct resonances around 0.4 THz, 0.6 THz, and 0.8 THz, respectively. The normal structure is composed of three different single-resonant circuits that have different capacitor-like gaps and inductive loops constructing three distinct LC resonances to realize the stop-bands around the resonant frequencies. In the complementary structure, according to Babinet's principle [37–39], if we rotate the polarization of electric field and magnetic field by 90 degree, the structure can realize the pass-resonances [34–36]. Both theoretical and experimental results reveal that these two kinds of resonators exhibit three strong and narrow pass-band and stop-band resonances. Moreover, for the complementary structure, the

experimental transmission rates of the three resonant frequencies are 90%, 64% and 80%, which are very attractive values in present. Applying this symmetric structure, THz multiple band-pass or band-stop filters and THz multiple frequency selectors may be realized.

2. NORMAL SYMMETRIC THREE-RESONANCE RESONATOR (STRR)

The geometry of this structure is strictly symmetric. Each side of it has three ELC-resonators. The middle resonators are closed circuits, and the outmost is an open resonant circuit. The designed symmetric three-resonant unit is shown in Figure 1(a), and the structure is constructed on 500 µm silicon substrate, with a relative permittivity of 11.9. The 300-nm-thick metal of the structure is made of Aluminum, with a conductance of 3.72×10^7 S/m. To fabricate the metal resonator, the Aluminum film is deposited on one side of silicon and then patterned into the designed shape by photo etching. The photographs of a portion of the fabricated structure are shown in Figure 1(b). The size parameters are the following: $a = 139.67\,\mu m$, $a_1 = 19.88\,\mu m$, $a_2 = a_3 = 14.91\,\mu m$, $a_4 = 12.01\,\mu m$, $b = 100.1\,\mu m$, $l_1 = 28.98\,\mu m$, $l_3 = 4\,\mu m$, $w = 61.11\,\mu m$, $w_1 = w_2 = w_3 = 4.98\,\mu m$, and $w_l = 4.97\,\mu m$.

Then, applying the 3D EM field commercial simulation software CST, the simulations with a finite difference time domain (FDTD) code have been carried out to study the resonant characteristics of the STRR. The results show that the surface current stimulated by the line

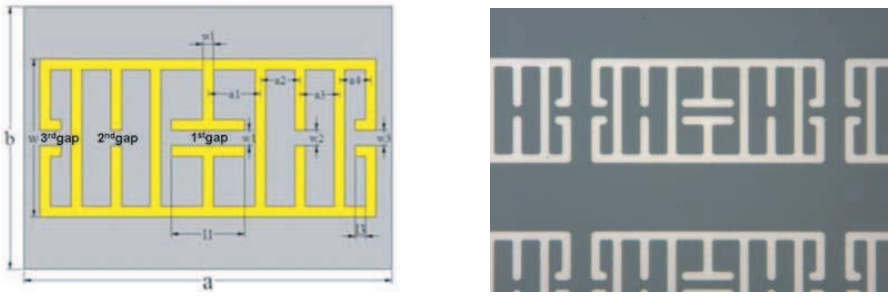

(a) (b)

Figure 1. Symmetric three-resonance resonator (a) designed three-resonant unit cell, with geometries: $a = 140\,\mu m$, $a_1 = 20\,\mu m$, $a_2 = a_3 = 15\,\mu m$, $a_4 = 12\,\mu m$, $b = 100\,\mu m$, $l_1 = 28\,\mu m$, $l_3 = 4\,\mu m$, $w = 60\,\mu m$, $w_1 = w_2 = w_3 = 6\,\mu m$ and $w_l = 4\,\mu m$. Thickness of Aluminum $t_1 = 0.3\,\mu m$, thickness of Silicon $t_2 = 500\,\mu m$. (b) Photomicrograph of a portion of the fabricated STRR.

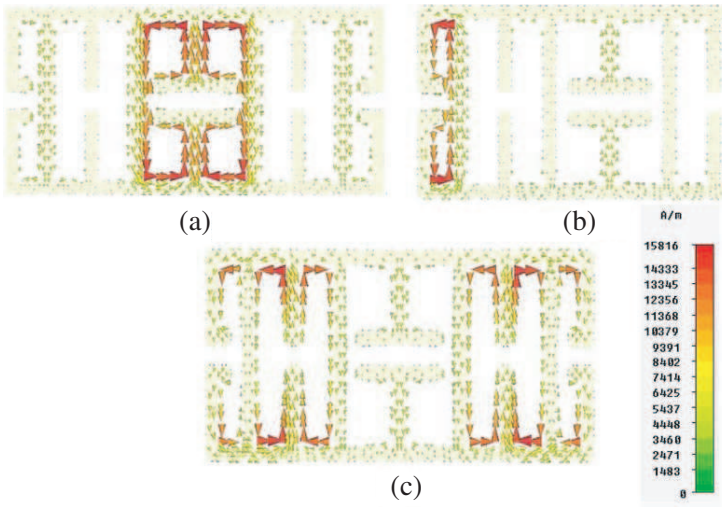

Figure 2. The circular surface current of designed STRR, corresponding to different resonant frequencies. (a) Near resonant frequency of 0.41 THz. (b) Near resonant frequency of 0.53 THz. (c) Near resonant frequency of 0.73 THz.

polarization incident wave in the structure has different characteristic distributions corresponding to different resonant frequencies, as demonstrated in Figure 2. It can also be found that there are three different resonant circuits. At 0.41 THz, the surface current mainly concentrates on the center circular loop (around the 1st gap). At the second resonant frequency 0.53 THz, surface current mainly flows through the middle circular loop (around the 2nd gap), and it concentrates on the outmost open circular loop (around the 3rd gap) near the highest resonant frequency 0.73 THz. The results demonstrate that the three circuits in the unit cause different equivalent LC resonances with different resonant frequencies. This complies with our anticipation that characteristics of its resonances are mainly determined by the equivalent capacity (gaps) and equivalent inductance (circuits) in the particle, which explains the appearance of minima in transmission. Moreover, the weak mutual coupling between different resonant parts within the unit also causes the distributions of surface current at resonant frequencies. The fields' distribution shown in Figure 3 also verifies these conclusions.

The experimental study of characterizing the performance of the resonators was performed using Terahertz time-domain spectroscopy (THz-TDS). For this experiment, a Ti:Sa femtosecond laser source

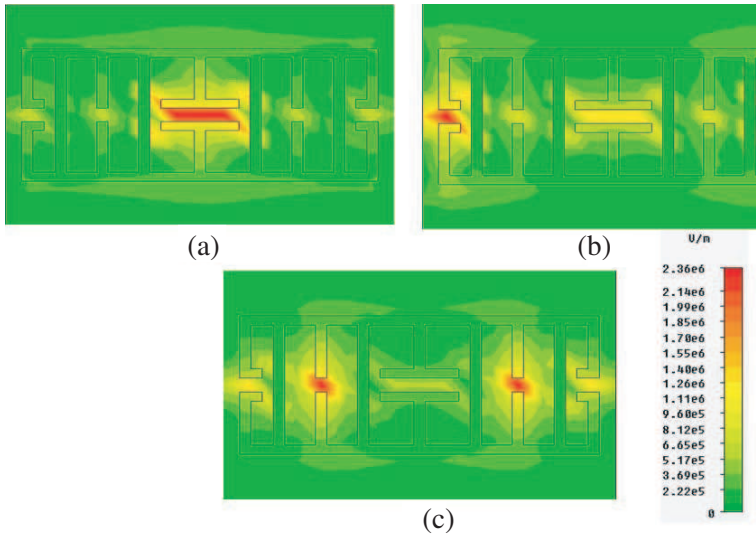

Figure 3. The electric field distribution of designed STRR, corresponding to different resonant frequencies. (a) Near resonant frequency of 0.41 THz. (b) Near resonant frequency of 0.53 THz. (c) Near resonant frequency of 0.73 THz.

delivering 80 fs pulses at 790 nm central wavelength is applied to the generation and detection of terahertz radiation. The excitation of the emitter with ultrashort laser pulses results in a burst of subpicosecond pulses with frequencies spanning from 0.1 THz to 3.0 THz terahertz. A polyethylene lens focuses the linearly polarized THz beam onto the metamaterial sample to a diameter of about 2 mm, and a second polyethylene lens recollimates the transmitted THz beam, which is directed to a photoelectric crystal. The Signal Noise ratio of this system is more than 1000.

The experiments were performed at room temperature 23 degrees in a dry air atmosphere. In THz-TDS, the time-varying electric field of the impulsive THz radiation is recorded, and the electric field spectral amplitude and phase are directly obtained by performing Fourier analysis. Measurements of this structure need to have a suitable reference, which, in this case, is a bare silicon substrate, allowing determination of the transmission as a function of frequency by dividing the Fourier transformed sample and reference waveforms. All the experiments are performed at normal linear polarization incidence with the THz electric and magnetic field lying in-plane. The polarization of the THz electric field is perpendicular to the split gaps as shown in Figure 4(a), and the transmission of the STRR obtained

is shown in Figure 4(d). Three transmission minima at 0.42, 0.56 and 0.79 THz are clearly observed. Compared with the measurement, the errors of the simulation for the minimum transmission frequencies are 2.4%, 5.7%, 8.2%, respectively.

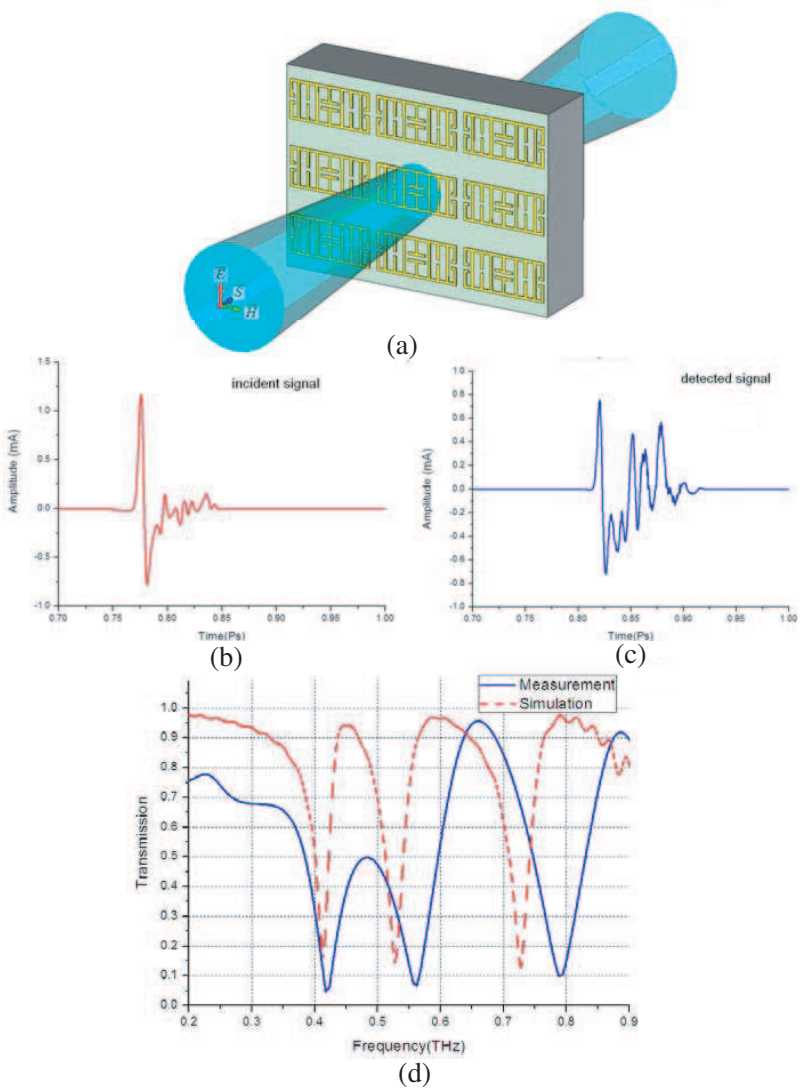

Figure 4. (a) The polarization of electric field and magnetic field. (b) Time domain waveforms of incident signal. (c) Time domain waveforms of detected signal. (d) Simulated (red line) and measured (blue line) transmissions of the resonator sample.

3. COMPLEMENTARY SYMMETRIC THREE-RESONANT RESONATOR (CSTR)

The structure of complementary symmetric three-resonant resonators (CSTR) is fabricated by the opposite processing technique on the surface of the silicon substrate. The blank area in the STRR now is covered with Aluminum. Correspondingly, the Aluminum patterns in the STRR will be hollowed out in the complementary structure as shown in Figure 5(a). The fabrication of complementary unit is shown in Figure 5(b). It can be found that the white areas are the Aluminum patterns, and the dark areas are blank where the silicon substrate can be observed directly.

Opposite to the STRR structure, in the CSTR, the metamaterial structure is hollow, so the fields and surface current excited by incident wave will concentrate in hollow area. As analysis above, in the normal STRR structure, the displacement current has been induced by time-varying incident wave in the gap between the metallic polar plates in metamaterial structure and then has formed the circulating currents in the circuits which can be equal to LC resonance. In CSTR, the resonant mechanism is different, because the three resonant passbands can only be induced by incident THz plane wave with perpendicular linear polarization (the polarization is rotated by 90° in the normal incident direction). In the STRR, the incident wave with (Ex, Hy) acts as an induced equivalent current shown in Figure 6(a). However, in CSTR, the perpendicular polarization wave (Hx, Ey) acts as the equivalent magnetic currents shown in Figure 6(b). According to the

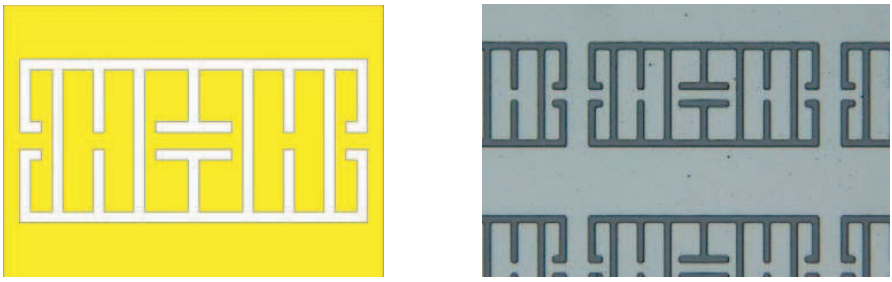

(a) (b)

Figure 5. Complementary symmetric three-resonant resonator. (a) A designed three-resonant unit cell. (b) Photomicrograph of a portion of the fabricated complementary symmetric three-resonant resonator.

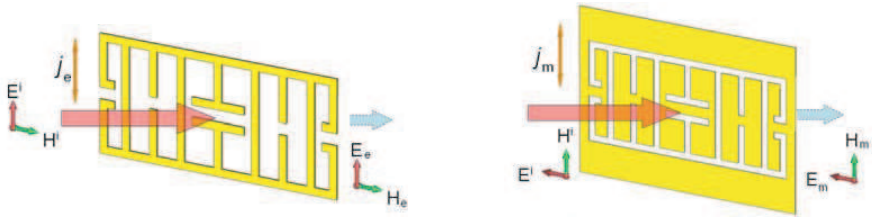

Figure 6. Equivalent element based on Babinet's principle. (a) Equivalent electric current of the STRR. (b) Equivalent magnetic currents of the CSTR.

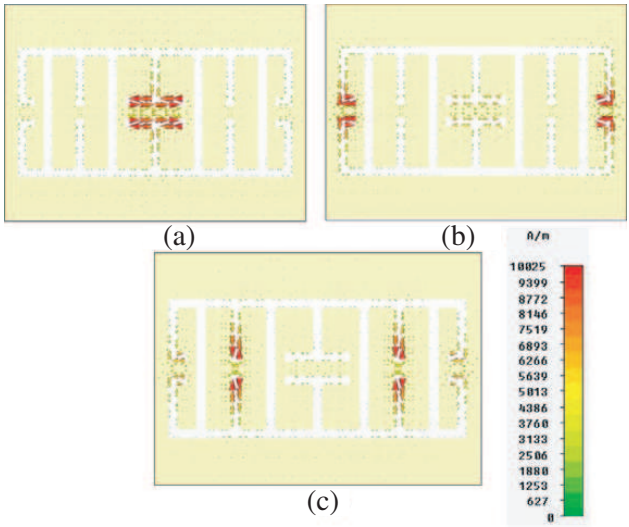

Figure 7. The circular surface current distribution of the designed CSTR near different resonant frequencies. (a) Near resonant frequency 0.43 THz. (b) Near resonant frequency 0.56 THz. (c) Near resonant frequency 0.81 THz.

Babinet's principle:

$$\begin{cases} E_m - Z_0 H_e = -Z_0 H^i \\ H_m + Z_0 E_e = Z_0 E^i \end{cases}$$

where $Z_0 = E^i/H^i$, then we can get: $\frac{E_m}{E^i} + \frac{E_e}{E^i} = 1$. So in the CSTR, the transmission will realize the passband at the resonant frequency.

Then the simulation is carried out. The surface current distribution shown in Figure 7 demonstrates that the circulating

currents cannot be induced. However, the parallel currents along the long side of the gap in the structure are excited. Figure 8 shows that similar to the electric fields distribution in STRR, the magnetic fields concentrate on the gaps. Around the lowest resonant frequency of 0.43 THz, the magnetic fields concentrate on the center gap, and of 0.56 THz, mainly on the outmost gaps and around the middle gaps corresponding to 0.81 THz. It should be emphasized that the flow direction of the surface currents are the same, i.e., along the long side of the gaps. Above results indicate that the fundamental mode is established in the slits of the gaps, so the transmission is caused by the nano-aperture resonance similar to the aperture-array transmission.

Finally, the experiments with THz-TDS have been implemented. The polarization of the THz electric fields was parallel to the split gaps shown in the Figure 9(a). The experimental results shown in Figure 9(b) demonstrate that there are three passbands around the resonant frequency: 0.41 THz, 0.60 THz and 0.86 THz. And the errors of the measurement for the transmission frequencies are 4.7%, 7.1% and 6.2%, respectively. The experimental results agree well with the simulation ones, demonstrating that this CSTR can realize the three-

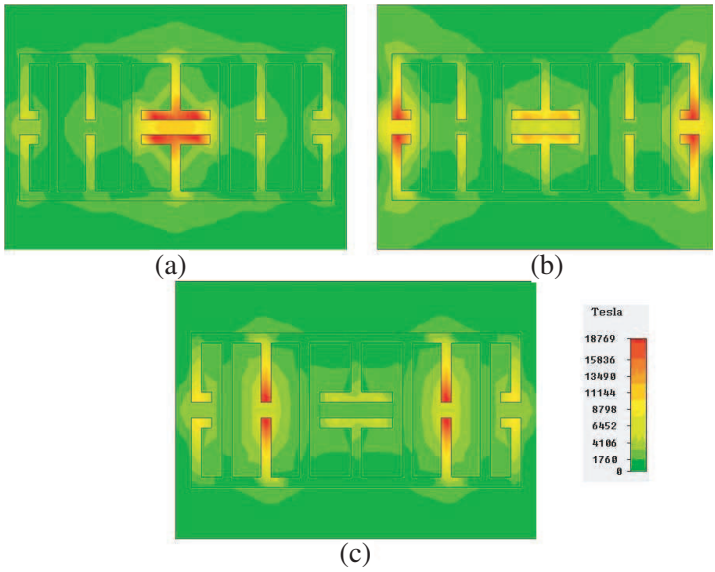

Figure 8. The magnetic field distribution of designed CSTR near different resonant frequencies. (a) Near resonant frequency of 0.43 THz. (b) Near resonant frequency of 0.56 THz. (c) Near resonant frequency of 0.81 THz.

passband function.

However, there are differences between the experimental results and those of simulation. Firstly, as shown in Figure 4 and Figure 9 there is a frequency shift which may be caused by fabrication

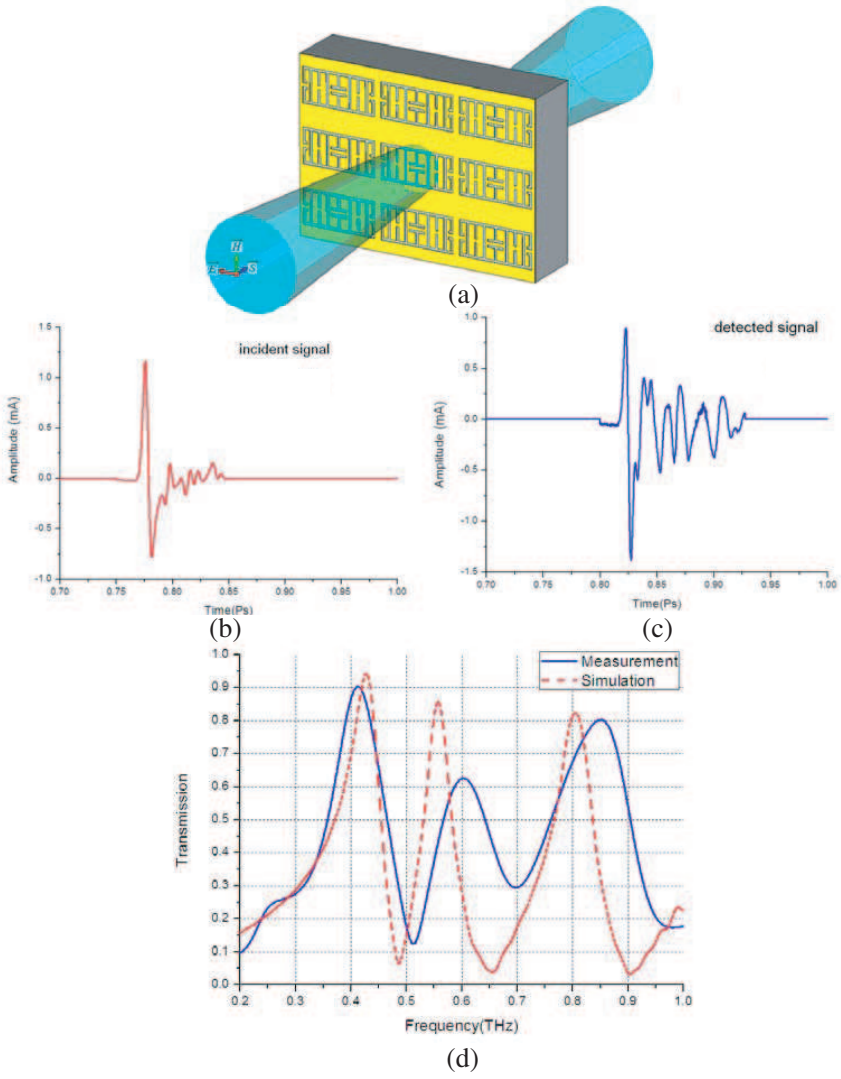

Figure 9. (a) The incident direction of electric field and magnetic field. (b) Time domain waveforms of incident signal. (c) Time domain waveforms of detected signal. (d) Simulated (red line) and measured (blue line) transmissions of the resonator sample.

tolerances and the boundary condition setting in simulation. In the fabrication, there is 0.5–1.0 µm mismachining tolerance. As we know, the resonances are induced by the equivalent LC resonant-circuits; the gaps act as the equivalent capacities; the lines are equal to inductance. So the mismachining tolerance causes the differences of the width of the gaps w_1, w_2, w_3 and the lines w_l between simulation and reality, which is the key factor leads to the frequency shift. On the other hand, in the simulation, considering the number of mesh and computing duration, only 10×10 array has been modeled. Moreover, ideal plane wave and open space boundary have been applied. In the experiment, the ideal boundary condition and incident plane wave cannot be fulfilled, and the number of units is larger than the model in simulation.

Secondly, the errors of transmission rates are due to the silicon substrate we use and the depth of the coated 300-nm-thick metal surface. In the simulation, ideal material factors have been used in the modeling. However, in the measurement, there are minor differences in the material factors of silicon substrate and the mismachining tolerance in the process of coating film (about 10 nm) which leads to the errors.

4. CONCLUSIONS

In summary, based on the structure of metamaterials, we present the study on the planar multi-band resonators by analyzing normal symmetric three-resonant resonator and the complementary structure. The study shows that the transmission of resonant frequencies in the normal structure is below 10%, while more than 80% of the transmission occurs in the complementary structure. According to our research, the experimental results showe good agreement with the simulation with slightly small difference in terms of resonant frequencies. This shows that the structure design features are clean and the resonant bands well-separated. The concept of this structure can be extended to realize multi-band metamaterials with more than 5 resonant frequencies.

Eventually, inspired by the idea reported in this paper, it can be predicated that the 2-D planar metamaterial fabricated on Silicon substrate will have many potential applications in the THz functional components, including multi-band filters, multi-resonant absorbers, sensors, etc. in the future.

ACKNOWLEDGMENT

This work is supported by the National Natural Science Foundation of China under Contract Nos. 61001031 and 61072036.

REFERENCES

1. Chen, H. T., W. J. Padilla, J. M. O. Zide, A. C. Gossard, A. J. Taylor, and R. D. Averitt, "Active terahertz metamaterial devices," *Nature*, Vol. 444, 597, 2006.
2. Oraizi, H., A. Abdolali, and N. Vaseghi, "Application of double zero metamaterials as radar absorbing materials for the reduction of radar cross section," *Progress In Electromagnetics Research*, Vol. 101, 323–337, 2010.
3. Sajin, G. I., "Impedance measurement of millimeter wave metamaterial antennas by transmission line stubs," *Progress In Electromagnetics Research Letters*, Vol. 26, 59–68, 2011.
4. Veselago, V. G., "The electrodynamics of substances with simultaneously negative values of ε and μ," *Sov. Phys. Usp.*, Vol. 10, 509, 1968.
5. Wu, Z., B. Q. Zeng, and S. Zhong, "A double-layer chiral metamaterial with negative index," *Journal of Electromagnetic Waves and Applications*, Vol. 24, No. 7, 983–992, 2010.
6. Smith, D. R., W. J. Padilla, D. C. Vier, S. C. Nemat-Nasser, and S. Schultz, "Composite medium with simultaneously negative permeability and permittivity," *Phys. Rev. Lett.*, Vol. 84, 4184, 2000.
7. Valagiannopoulos, C. A., "Electromagnetic scattering of the field of a metamaterial slab antenna by an arbitrarily positioned cluster of metallic cylinders," *Progress In Electromagnetics Research*, Vol. 114, 51–66, 2011.
8. Shelby, R. A., D. R. Smith, and S. Shultz, "Experimental verification of a negative index of refraction," *Science*, Vol. 292, 77, 2001.
9. Butt, H., Q. Dai, T. D. Wilkinson, and G. A. J. Amaratunga, "Photonic crystals & metamaterial filters based on 2D arrays of silicon nanopillars," *Progress In Electromagnetics Research*, Vol. 113, 179–194, 2011.
10. Yuan, Y., L. Ran, H. S. Chen, J. Huangfu, T. M. Grzegorczyk, and J. A. Kong, "Backward coupling waveguide coupler using left-handed material," *Appl. Phys. Lett.*, Vol. 88, 211903, 2006.
11. Bucinskas, J., L. Nickelson, and V. Shugurovas, "Microwave scattering and absorption by a multilayered lossy metamaterial — Glass cylinder," *Progress In Electromagnetics Research*, Vol. 105, 103–118, 2010.
12. Chen, H. S., B. I. Wu, L. Ran, T. M. Grzegorczyk, and J. A. Kong, "Controllable left-handed metamaterial and its application to a

steerable antenna," *Appl. Phys. Lett.*, Vol. 89, 053509, 2006.

13. Sabah, C. and S. Uckun, "Multilayer system of Lorentz/Drude type metamaterials with dielectric slabs and its application to electromagnetic filters," *Progress In Electromagnetics Research*, Vol. 91, 349–364, 2009.
14. Withayachumnankul, W. and D. Abbott, "Metamaterials in the terahertz regime," *IEEE Photonics Journal*, Vol. 1, 99, 2009.
15. Rahimi, H., A. Namdar, S. Roshan Entezar, and H. Tajalli, "Photonic transmission spectra in one-dimensional fibonacci multilayer structures containing single-negative metamaterials," *Progress In Electromagnetics Research*, Vol. 102, 15–30, 2010.
16. Zhao, X., L. Zhao, K.-M. Huang, and C.-J. Liu, "A circularly polarized array composed of linear polarized microstrip patches fed by metamaterial transmission line," *Journal of Electromagnetic Waves and Applications*, Vol. 25, No. 11–12, 1545–1553, 2011.
17. Tao, H., N. L. Landy, C. M. Bingham, X. Zhang, R. D. Averitt, and W. J. Padilla, "A metamaterials absorber for the terahertz regime: Design, fabrication and characterization," *Opt. Express*, Vol. 16, 007181, 2008.
18. Zhou, H., F. Ding, Y. Jin, and S. L. He, "Terahertz metamaterial modulators based on absorption," *Progress In Electromagnetics Research*, Vol. 119, 449–460, 2011.
19. Chen, H. T., W. J. Padilla, J. M. O. Zide, S. R. Rank, A. C. Gossard, A. J. Taylor, and R. D. Averitt, "Ultrafast optical switching of terahertz metamaterials fabricated on ErAs/GaAs nanoisland superlattices," *Opt. Lett.*, Vol. 32, 001620, 2007.
20. Kuznetsov, S. A., A. G. Paulish, A. V. Gelfand, P. A. Lazorskiy, and V. N. Fedorinin, "Matrix structure of metamaterial absorbers for multispectral terahertz imaging," *Progress In Electromagnetics Research*, Vol. 122, 93–103, 2012.
21. Zhu, B., Z. Wang, C. Huang, Y. Feng, J. Zhao, and T. Jiang, "Polarization insensitive metamaterial absorber with wide incident angle," *Progress In Electromagnetics Research*, Vol. 101, 231, 2010.
22. Chen, H. T., W. J. Padilla, M. J. Cich, A. K. Azad, R. D. Averitt, and A. J. Taylor, "A metamaterial solid-state terahertz phase modulator," *Nature Photonics*, Vol. 3, 148–151, 2009.
23. Zhang, Y. X., S. Qiao, W. X. Huang, W. Ling, and L. Li, "Asymmetric single-particle triple-resonant metamaterial in terahertz band," *Appl. Phys. Lett.*, Vol. 99, 073111, 2011.

24. Cai, M. and E. P. Li, "A novel terahertz sensing device comprising of a parabolic reflective surface and a bi-conical structure," *Progress In Electromagnetics Research*, Vol. 97, 61–73, 2009.
25. Padilla, W. J., A. J. Taylor, and C. Highstrete, "Dynamical electric and magnetic metamaterial response at terahertz frequencies," *Phys. Rev. Lett.*, Vol. 96, 107401, 2006.
26. Guo, Y. and R. Xu, "Planar metamaterials supporting multiple left-handed modes," *Progress In Electromagnetics Research*, Vol. 66, 239–251, 2006.
27. Azad, A. K., A. J. Taylor, E. Smirnova, and J. F. O'Hara, "Characterization and analysis of terahertz metamaterials based on rectangular split-ring resonators," *Appl. Phys. Lett.*, Vol. 92, 011119, 2008.
28. Tang, M. C., S.-Q. Xiao, T. Deng, D. Wang, and B.-Z. Wang, "A dual-band epsilon-negative material design using folded-wire structures," *Journal of Electromagnetic Waves and Applications*, Vol. 25, No. 2–3, 327–337, 2011.
29. Cao, W.-Q., B. N. Zhang, T. B. Yu, A. J. Liu, S. J. Zhao, D. S. Guo, and Z. D. Song, "Single-feed dual-band dual-mode and dual-polarized microstrip antenna based on metamaterial structure," *Journal of Electromagnetic Waves and Applications*, Vol. 25, No. 13, 1909–1919, 2011.
30. Yuan, Y., C. Bingham, T. Tyler, S. Palit, T. H. Hand, W. J. Padilla, D. R. Smith, N. M. Jokerst, and S. A. Cummer, "Dual-band planar electric metamaterial in the terahertz regime," *Opt. Express*, Vol. 16, 9746–9752, 2008.
31. Yuan, Y., C. Bingham, T. Tyler, S. Palit, T. H. Hand, W. J. Padilla, D. R. Smith, N. M. Jokerst, and S. A. Cummer, "A dual-resonant terahertz metamaterial based on single-particle electric-field-coupled resonators," *Appl. Phys. Lett.*, Vol. 93 191110, 2008.
32. Huang, L. and H. Chen, "Multi-band and polarization insensitive metamaterial absorber," *Progress In Electromagnetics Research*, Vol. 113, 103–110, 2011.
33. Wang, J. F., S. B. Qu, Y. M. Yang, H. Ma, X. Wu, and Z. Xu, "Multiband left-handed metamaterials," *Appl. Phys. Lett.*, Vol. 95, 014105, 2009.
34. Chen, H. T., J. F. O'Hara, A. J. Taylor, R. D. Averitt, C. Highstrete, M. Lee, and W. J. Padilla, "Complementary planar terahertz metamaterials," *Opt. Express*, Vol. 15, 001084, 2007.

35. Rockstuhl, C., T. Zentgraf, T. P. Meyrath, H. Giessen, and F. Lederer, "Resonances in complementary metamaterials and nanoapertures," *Opt. Express*, Vol. 16, 002080, 2008.
36. Hand, T. H., J. Gollub, S. Sajuyigbe, D. R. Smith, and S. A. Cummer, "Characterization of complementary electric field coupled resonant surfaces," *Appl. Phys. Lett.*, Vol. 93, 212504, 2008.
37. Edmunds, J. D., M. C. Taylor, A. P. Hibbins, J. R. Sambles, and I. J. Youngs, "Babinet's principle and the band structure of surface waves on patterned metal arrays," *J. Appl. Phys.*, Vol. 107, 103108, 2010.
38. Bitzer, A., A. Ortner, H. Merbold, T. Feurer, and M. Walther, "Terahertz near-field microscopy of complementary planar metamaterials: Babinet's principle," *Opt. Express*, Vol. 19, 002537, 2011.
39. Zentgraf, T., T. P. Meyrath, A. Seidel, S. Kaiser, H. Giessen, C. Rockstuhl, and F. Lederer, "Babinet's principle for optical frequency metamaterials and nanoantennas," *Phys. Rev. B*, Vol. 76, 033407, 2007.